Graphical Abstract

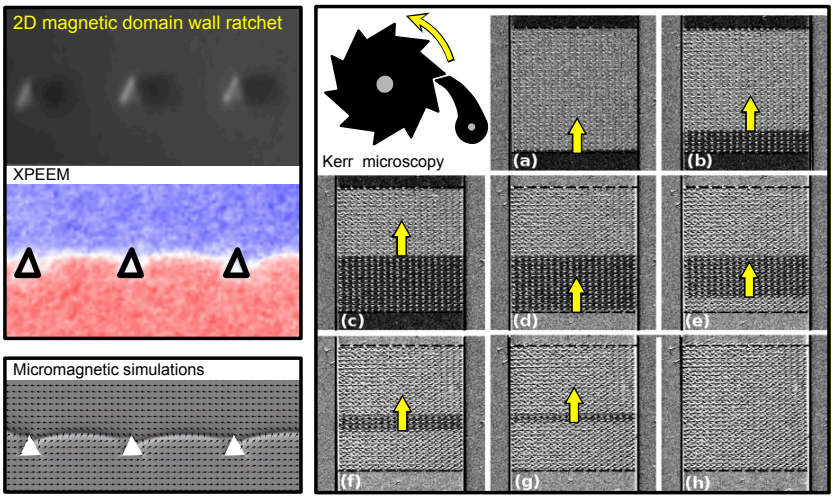

Highlights

- Ratchet and crossed-ratchet effects in magnetic domain wall motion through 2D arrays of asymmetric submicrometric holes have been achieved.
- Micromagnetic simulations and high-resolution magnetic imaging show that in the submicrometric size regime domain walls become stiff, influencing their propagation.
- Half vortex topological charge at the perimeter of the holes results in the asymmetric shape and propagation of the domain walls.
- Simulations predict the control of an asymmetric propagation of domain walls in two opposite directions with electrical currents and magnetic fields.

2D magnetic domain wall ratchet: the limit of submicrometric holes

J. Herrero-Albillos[a,b,c], C. Castán-Guerrero[b,c], F. Valdés-Bango[d,e], J. Bartolomé[b,c], F. Bartolomé[b,c], F. Kronast[f], A. Hierro-Rodriguez[g], L. M. Álvarez Prado[d,e], J. I. Martín[d,e], M. Vélez[d,e], J. M. Alameda[d,e], J. Sesé[h,c], L. M. García[b,c]

[a] *Centro Universitario de la Defensa, Zaragoza, Spain*
[b] *Instituto de Ciencia de Materiales de Aragón (ICMA), CSIC – Universidad de Zaragoza, Zaragoza, Spain*
[c] *Dpto. de Física de la Materia Condensada, Universidad de Zaragoza, Zaragoza, Spain*
[d] *Departamento de Física, Universidad de Oviedo, 33007 Oviedo, Spain*
[e] *Centro de Investigación en Nanomateriales y Nanotecnología, CINN (CSIC – Universidad de Oviedo), 33940 El Entrego, Spain*
[f] *Helmholtz-Zentrum Berlin für Materialien und Energie GmbH, 12489 Berlin, Germany*
[g] *IN-IFIMUP / INESC-Porto, Faculdade de Ciencias, Universidade do Porto, Rua do Campo Alegre, 4169-007, Porto, Portugal*
[h] *Instituto de Nanociencia de Aragón (INA) and Laboratorio de Microscopías Avanzadas (LMA), Universidad de Zaragoza, Zaragoza, Spain*

Abstract

The study of ratchet and crossed-ratchet effects in magnetic domain wall motion through 2D arrays of asymmetric holes is extended in this article to the submicrometric limit in hole size (small size regime). Therefore, the gap has been closed between the 2D ratchets in the range of tens-of-micrometers (large size regime) and the small size regime 1D ratchets based on nanowires. The combination of Kerr microscopy, X-Ray PhotoEmission Electron Microscopy and micromagnetic simulations has allowed a full magnetic characterisation of both the domain wall (DW) propagation process over the whole array and the local DW morphology and pinning at the holes. It is found that the 2D small size limit is driven by the interplay between DW elasticity and half vortex propagation along hole edges: as hole size becomes comparable to DW width, flat DW propagation modes are favoured over kinked DW propagation due to an enhancement of DW stiffness, and pinned DW segments adopt asymmetric configurations related with Néel DW chirality. Nevertheless, both ratchet and crossed-ratchet effects have been experimentally found, and we propose a new ratchet/ inverted-ratchet effect in the submicrometric range driven by magnetic fields and electrical currents respectively.

Keywords: Magnetic Ratchet effect, Domain Wall, Pinning, Domain Wall Chirality,

1. Introduction

The control of magnetic domain walls (DWs) is a problem of great current interest for the nanomagnetics research community. The development of novel devices, such as racetrack memories[1, 2, 3] or domain wall logic based systems,[4, 5, 6, 7] is based on the creation and propagation of DWs. New advances will only come through the fundamental understanding of magnetic DW dynamics in restricted geometries, which requires a deep insight into complex 2D interfaces.

Of particular interest is the ratchet effects that are induced by an asymmetry in the propagation direction of DWs, since they open the door to the design of spintronics devices[8, 9] like magnetic DW diodes [10, 11] and shift registers.[6, 12, 13] Progress in this field can also inspire the research in asymmetric motion of ferroelectric DWs,[14] skyrmions[15] or vortices in superconductors.[16]

Magnetic ratchet effect has been studied in different geometries, from extended 2D magnetic films to magnetic nanowires, dots or even two-dimensional electron gases.[10, 17, 18, 19, 20] Different mechanisms have been demonstrated to favour asymmetric DW motion, such as shape anisotropy in an asymmetric geometry,[10, 17, 18, 21] anisotropy gradients created by nonuniform irradiation profiles,[12] asymmetric stray field configurations,[22] Dzyaloshinskii-Moriya interactions in ultra-thin films,[23] or asymmetric DW pinning potentials created by the interaction between

*Corresponding author
Email address: Julia.Herrero@unizar.es
(J. Herrero-Albillos)

sample geometry and internal DW structure.[24]

Patterning into an asymmetric configuration has been one of the preferred options to create magnetic DW ratchets. However, depending on sample dimensions relative to DW width, very different mechanisms are at the origin of the observed ratchet effects. Examples of patterns with small dimensions compared with the DW width (i.e. small size regime), can be found in the asymmetric motion of magnetic DWs through nanowires with a triangular structure [10] or asymmetric notches.[25] The studied nanowires are narrow enough to be considered unidimensional, and thus the DWs behave essentially as point particles in a 1D asymmetric potential created by the changes in DW energy and configuration across the notched structure.[24]

In the opposite limit, archetype of the large size regime are the studies of DW motion across 2D arrays of asymmetric holes with large dimensions (i.e. $\geq 10\ \mu$m) compared with the DW width.[17, 26, 27] In this case, DWs can be approximated as elastic lines of zero width that can distort throughout their length in response to the 2D asymmetric pinning potential.[28] The motion of these DWs can be quite complex. In particular, the so-called crossed-ratchet effect can be observed: the preferred direction for DW motion can have two opposite directions depending on the applied magnetic field, the geometrical parameters and, more importantly, the shape of the domain wall within the 2D array (flat or kinked). Interestingly, micromagnetic simulations suggest that the optimum hole size for this effect would be twice the DW width, that is $\sim 1\ \mu$m holes for the amorphous Co-Si alloys reported in Ref. [26].

To date, there are no comprehensive experimental results in such small sizes and hence, the aim of the present work is to extend the study of DW propagation in 2D arrays of asymmetric holes to the micrometric regime to unravel the ratchet and crossed-ratchet effects. Additionally, this study closes the gap between the small (1D nanowires) and large (2D arrays of holes) regimes already found in the literature. For this purpose, arrays of triangle-shaped holes have been fabricated with triangle sizes comparable to the DW width in amorphous Co-Si alloys. The propagation modes, pinning and domain wall morphology have been investigated by means of two complementary magnetic imaging techniques: wide field Kerr microscopy and high resolution X-Ray Photoemission Electron Microscopy (XPEEM). The experimental results have been compared with micromagnetic simulations. The small size regime is found to be marked by a reduction of DW elasticity and by an increasing relevance of edge propagation asymmetries related to Néel DW chirality (i.e. sense of magnetisation rotation). Additionally, micromagnetic simulations of the current induced DW propagation suggest the occurrence of an inverted ratchet effect.

2. Methods

2.1. Sample fabrication

Amorphous $Co_{0.7}Si_{0.3}$ have been deposited on Si(100) substrates by means of Co and Si co-sputtering as reported elsewhere.[29] The films -30 nm thick- have a well defined uniaxial anisotropy, with an in-plane magnetisation easy axis (EA) defined by the deposition direction. Reversal of the film magnetisation takes place mainly by the propagation of Néel type DWs laying parallel to the EA.

Arrays of triangle-shaped holes have been fabricated on the films by means of electron beam lithography (EBL) followed by an argon ion milling step.[30] The base of the triangles (displayed as horizontal in the figures unless otherwise stated) have been fabricated both parallel and with a 13° tilt with respect to the EA of the film, with all the tips in each particular array either pointing up or down. The total area covered by each array is a 60 μm side square with two 50

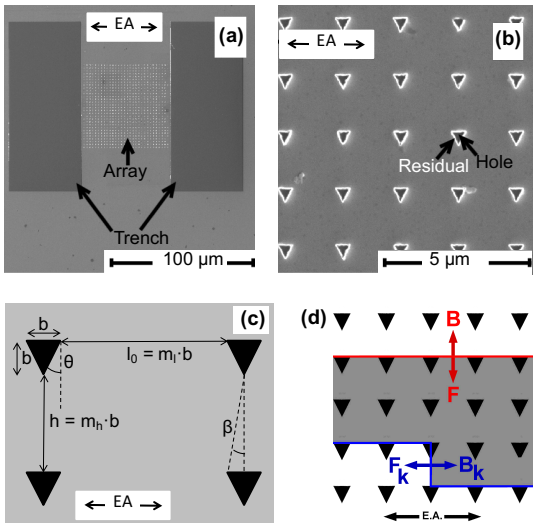

Figure 1: (a) SEM top-view image covering a whole array and the two trenches. (b) SEM image of a portion of the array with triangle-shaped holes, $m_l = m_h = 4$ and $b = 500$ nm. (c) Scheme of the geometrical parameters of the arrays as defined in the main text. θ and β are the angles defined in Ref. [28], taking the values $\theta = 26.5°$ and $\beta = 5.7°$, 7.1° and 9.5° for this work. (d) Scheme of the possible propagation directions of a flat DW (red flat line) and a kinked DW (blue kinked line). F/B: Forward/Backward flat DW propagation modes; F_k/B_k: Forward/Backward kinked DW propagation modes.

μm wide trenches, in which the magnetic material has been removed to create a channel for the DWs. Fig. 1 shows scanning electron microscopy (SEM) image of one complete array and a zoomed area. Some residual electron sensitive resist (PMMA) from the EBL process could not be fully removed, but it is not expected to significantly affect the magnetic measurements.

The base and height of the triangles have the same size, b, with $b = 500$ nm and 1 μm (see Fig. 1(c)). The column (l_0) and row (h) separations have been chosen to be multiples of b, i.e. $l_0 = m_l \cdot b$ and $h = m_h \cdot b$, with m_l and m_h factors taking the values 3, 4 and 5. In order to compare the observations between the symmetric and asymmetric cases, an array of rhomb-shaped holes, with $b = 500$ nm and $m_l = m_h = 4$ has been fabricated, and the results can be seen in the supplementary material.[1]

In order to design the array geometries we have taken as starting point the model for propagation of elastic interfaces across rectangular arrays of triangular holes used in previous studies,[28] In this framework, the chosen triangle aspect ratio and inter hole distances correspond to a regime that favours flat DW propagation in the forward direction (F mode, propagation field H_F) and kinked DW backward propagation (B_k mode, propagation field H_B^k), as defined in Fig. 1(d).

2.2. Magnetic characterisation

Two different imaging techniques have been used for the magnetic characterisation of the samples: Kerr microscopy and X-ray PhotoEmission Electron Microscopy (XPEEM).

Images of the complete arrays have been obtained with a wide field Kerr effect microscope from Evico Magnetics GmbH, operating in longitudinal configuration. A magnetic field has been applied in plane parallel to base of the triangles. Live videos of the DW propagation across each array have been recorded while changing the applied magnetic field. The temporal resolution of the camera is 16 fps, which is sufficient for observing the propagation of DWs moving at an average speed slower than 1 μm/s. The light-grey and dark-grey areas in the images relate to magnetisation parallel and antiparallel to the applied magnetic field respectively.

DW morphology and local pinning at the holes has been imaged by means of XPEEM at the UE49-PGM-1-SPEEM beamline of the BESSY II synchrotron (HZB, Berlin). The magnetic contrast is obtained by using X-ray Magnetic Circular Dichroism (XMCD) at the Co L_3 X-ray absorption edge, applying the standard data treatment.[31] XMCD images of a fraction of the arrays are obtained with resolution of around 30 nm, where the signal (represented in red-white-blue) is proportional to the projection of the magnetisation along the direction of the incident X-ray beam (i.e. 16° angle of incidence measured from sample surface), and therefore mostly being sensitive to in-plane magnetisation along the beam. A magnetic sample holder has been used in order to apply a magnetic field during measurements.

2.3. Micromagnetic simulations

Micromagnetic simulations of the DW pinning and propagation through the arrays have been performed using the OOMMF code.[32] Several arrays of 4×4 empty triangular holes have been defined in a rectangular 30 nm thick film elements (so as to simulate the patterned film). Array geometry is the same as in Fig. 1 with b = 500 nm. Material parameters correspond to those of the Co-Si alloy: $M_S = 2 \cdot 10^5$ Am^{-1}, $A = 3 \cdot 10^{-11}$ J/m and uniaxial anisotropy $K = 1000$ J/m^3 [27] with the EA parallel to the isosceles triangle base. Mesh size 10 nm has been used, smaller than both the material exchange length, $\delta_{ex} = (2A/\mu_0 M_S^2)^{1/2} = 35$ nm, and the Bloch parameter $\delta_0 = (A/K)^{1/2} = 170$ nm.[27] Simulations start at a zero magnetisation state, with a Néel DW located in the middle of the array. Then, in order to obtain the critical fields for DW propagation, a magnetic field is applied along the EA, and increased in steps until DW propagation across the first line of triangular holes is achieved.

3. Results and Discussions

Magnetic characterisation has been performed in tens of square ($m_l = m_h$) and rectangular ($m_l \neq m_h$) arrays. As expected,[33] the introduction of the holes increases the coercivity of the arrays with respect to the unpatterned film (8 Oe according to Ref.[29], but values as low as 4 Oe are obtained in these samples). This can be clearly observed from the Kerr effect microscopy live videos: when reversing the magnetisation, switched domains first nucleate somewhere in the film and then grow until a DW gets pinned at the edge of the array. Further increasing the applied field results in the DW entering and propagating in the arrays. Full videos of selected examples can be seen in the supplementary material.

Results for the arrays aligned with the EA with the triangular holes pointing up and down and separations m_l and m_h equal to 3 and 5 are presented in subsection 3.1, and for square arrays tilted 13° with respect to the EA

[1] url to be introduced by the editor

with $m_l = 3, 4$ and 5 in subsection 3.2. Domain wall morphology and pinning is studied in subsection 3.3. Current induced domain wall propagation has been investigated by means of simulations, and the results for a square array with $b = 500$ nm and $m_l = 4$ are presented in subsection 3.4.

3.1. Flat domain wall propagation.

In the case of arrays fabricated with the triangular holes aligned with the EA, domain walls are always captured moving flat (horizontal in the images and videos), i.e. no kink propagation of DW occurs in these geometries. Figs. 2 and 3 show a series of photograms extracted from the videos of the arrays with triangles pointing down and up respectively, and with $b = 500$ nm, $m_l = 5$ and $m_h = 3$.

In the first example, a full hysteresis loop is performed, i.e. starting from positive saturation magnetisation of the whole array and the surrounding film (light grey in Fig. 2) the field is decreased and set negative until negative magnetisation (dark grey) is reached. A magnetic field of -20 Oe is then applied in order to ensure magnetic saturation. After that, an equivalent switching process is reproduced for positive applied magnetic fields. During all the process, only one domain wall at a time is seen within the array, always propagating down (↓) regardless of the sign of the applied magnetic field. As defined in Fig. 1, this corresponds to the forward direction (F) for triangles pointing down.

A minor loop is performed in the equivalent array with the triangles pointing up (in this case the F direction corresponds with a upwards propagation (↑)), as shown in Fig. 3. For this experiment, starting from positive saturation, the field is decreased, triggering the movement of a DW in the F direction. Once the DW is approximately half way into the array, the magnetic field is switched. This same DW is unable of propagating in the B direction and stays pinned. Therefore another DW, entering the array in the F direction from the unpatterned film, completes the magnetisation switching process.

As seen so far, DWs always propagate in the F direction (e.g. down for Fig. 2 and up for Fig. 3) regardless of the sign of the applied magnetic field or the orientation of the triangles (up or down), demonstrating the ratchet effect in DW motion is caused by the asymmetric shape of the holes.[2]

[2] A further proof of the ratchet effect originating from the asymmetric shape of the holes is presented at the supplementary material, where similar experiments as the ones described here show that DW propagation through arrays with symmetric holes respect to the DW propagation happens in both the F and B direction.

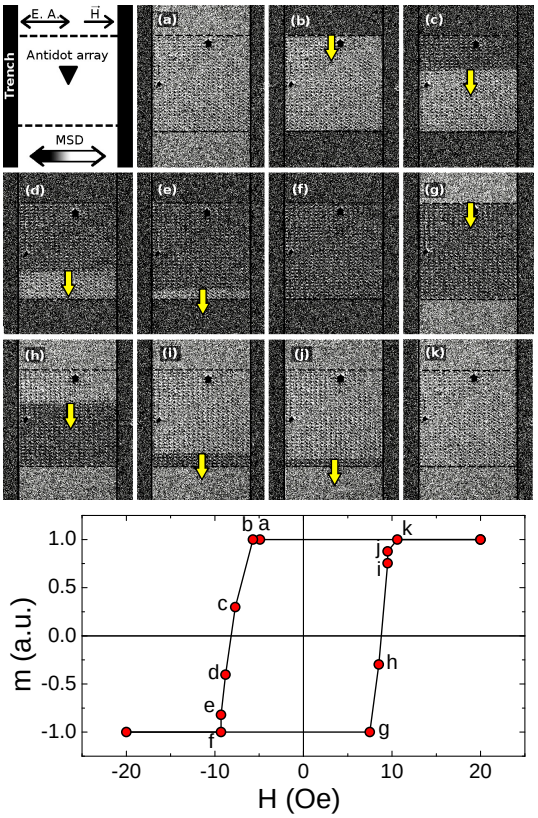

Figure 2: Kerr microscopy images of the array with $b = 500$ nm, $m_l = 5$, $m_h = 3$ and triangles pointing downwards (F direction: ↓), along a magnetic hysteresis loop. Yellow vertical arrows indicate the position and propagation direction of DW. The horizontal colour-faded arrow indicates the magnetic sensitivity direction (MSD) as parallel (light grey) and antiparallel to positive field (dark grey). The direction of the applied field and the EA are also sown as thin arrows. The array magnetisation can be extracted from the photograms as a function of the applied field, as shown in the lower panel, where the letters a to k label the magnetisation of each of the subfigures above.

For each magnetisation process, only the lower critical DC field for DW propagation can be determined experimentally, and therefore the critical fields for kinked DW propagation or backward DW propagation cannot be resolved for the so far studied arrays. The critical field for flat forward DW propagation, H_F, is rather a distribution than a single value since it does not only depends on the array geometry (e.g. m_l or m_h) but also depends on several effects: inhomogeneities in the holes shape and size, DW dynamics,[34, 35] field change rate, attractive/repulsive forces between pairs of Néel DWs,[36] DW velocity,[37] as well as intrinsic stochastic pinning.[38, 39, 40, 41] Inset of Fig. 4 shows the magnetic field range at which DW movement has been observed in the videos. The minimum val-

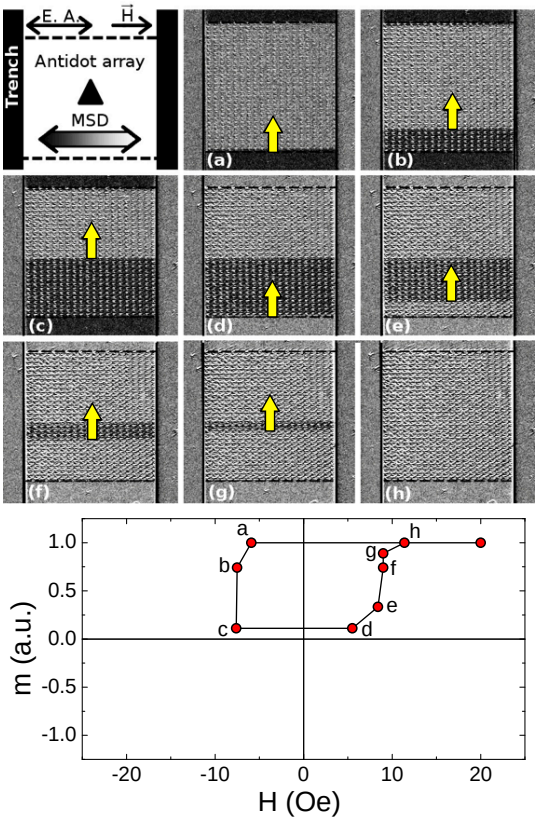

Figure 3: Kerr microscopy images of the array with $b = 500$ nm, $m_l = 5$, $m_h = 3$ and triangles pointing upwards (F direction: ↑), along a minor hysteresis loop. Yellow arrows indicate the propagation direction of DWs. Lower panel: magnetisation of the array as a function of the applied field extracted from the photograms.

ues, H_{min}, correspond to the depinning field for the first row of the arrays which, from the simple elastic theory approximation,[28] should scale with the inverse of inter-hole distance (i.e. with the inverse of l_0). Main Fig. 4 shows the H_{min} vs. $1/l_0$ together with a fit to a straight line, showing that this depinning field has two contributions: the coercive field of the continuous film (4.7 Oe from the fit) and the aforementioned dependence with $1/l_0$.

In summary, flat DW propagation shows a clear ratchet effect, originated only by the asymmetric shape of the holes, since the easy DW propagation direction, defined as F, is coincident with the direction in which the triangles point. The critical field for F propagation has been observed to decrease with increasing inter-hole distances but cannot be compared with the equivalent field for B propagation or for kinked propagation, since the related DW movement has not been observed.

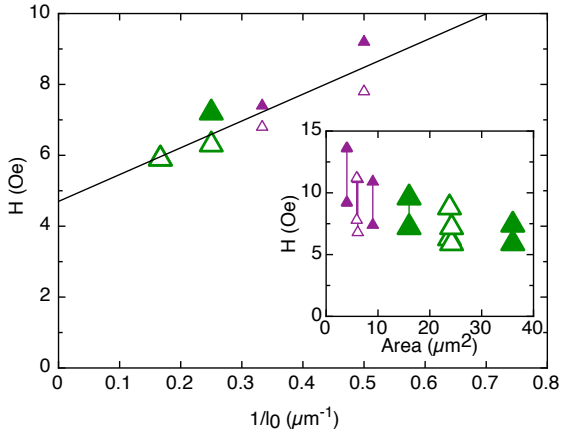

Figure 4: Minimum field for F propagation, as a function of the inverse of inter-hole separation. Continuous line is a fit to a straight line, where the intersection with the vertical axis returns the coercive field of the continuous film. Full triangles correspond to square arrays, open symbols to rectangular, small symbols to $b = 500$ nm and big symbols to 1 μm. m_l and m_h take values 3 and 5. Inset: magnetic field ranges at which the F propagation has been observed in arrays aligned parallel to the EA as a function of the cell area $[(l_0+b)(h+b)]$.

3.2. *Kinked domain wall propagation.*

The absence of crossed-ratchet effect in the arrays with their EA parallel to the triangles bases is not surprising since they do not present kink nucleation and propagation of DWs, which is known to be a prerequisite for its occurrence. In the crossed-ratchet mode, F propagation should occur for flat walls while B_k propagation should take place for kinked walls.[17, 28] Previous theoretical studies predicted kink propagation to be the softer DW propagation mode for those geometries,[26, 28] but always starting from an initial configuration in which the kink was already nucleated. Therefore, in order to experimentally observe the crossed-ratchet effect, the nucleation of kinks was favoured by fabricating a set of arrays with a small misalignment (13°) with respect to the magnetic EA of the film. This is expected to cause the DWs to enter tilted into the array, therefore facilitating the nucleation of kinks. In addition, since the magnetic field is also applied 13° tilted respect to the magnetic EA, there is a small transversal component of the field, which was already proven to favour kink propagation. [27]

Indeed, when such an array is produced, kinks do nucleate and propagate, as shown in Fig. 5, where selected Kerr microscopy images for a square array of triangles pointing up, with size $b = 1$ μm, and separation $m_l = 3$, are shown. In the images the yellow arrows indicate the evolution of kinks, which produce a B_k (↓) movement of the DW as indicated in Fig. 1. It has to be noted

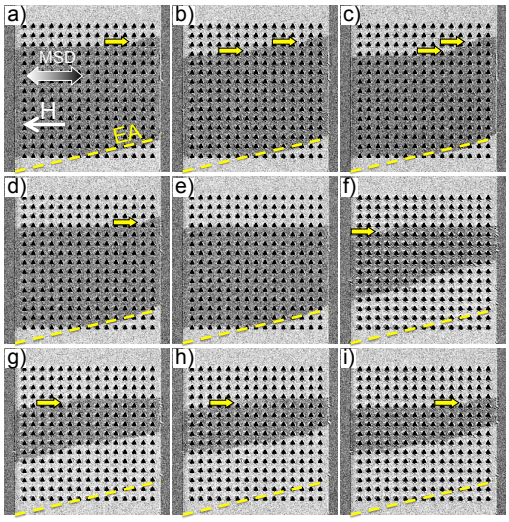

Figure 5: Kerr microscopy images in an array 13° tilted with respect to the EA, with $b = 1$ μm, $m_l = m_h = 3$ and triangles pointing up. The evolution of kinks has been marked with yellow arrows. The applied field (white arrow) is parallel to the hole rows, i.e. 13° tilted with respect to the EA (yellow dashed line). The triangle geometry has been plotted on top of the images for the sake of clarity

that the kinks are nucleated always at the left limit of the array and propagated towards the right limit, which is probably an indicator of the chirality of the DW. In addition, a DW parallel to the EA (i.e. forming a 13° angle with the horizontal) simultaneously propagates in the F direction (↑). The yellow dashed lines in Fig. 5 indicate the direction of the EA as well as the overall direction of the wall as it propagates, which can be considered roughly flat. Therefore, this observation may be classified as a crossed-ratchet effect.

Surprisingly, no kinks were observed in square arrays with $b = 1$ μm and larger separation (i.e. $m_l = 5$), whereas they were frequently observed in tilted arrays of smaller holes size ($b = 500$ nm). The visualisation of kinks in the smaller arrays is more challenging (due to the limited resolution of the microscope) nonetheless a detailed analysis is presented in the supplementary material.

Elastic theory calculations predict a ratio of the order of 3 for H_F/H_B^k for square arrays with $b = 500$ nm and 1 μm and $m_h > 2$.[28] Since both F and B_K propagations are observed simultaneously in the studied arrays, the ratio H_F/H_B^k is, therefore, much closer to the unity than anticipated. The difference can be due to the influence of the coercive field of the film, since it is the largest contribution to the value obtained for the critical field for domain propagation (both F and B^k), but also to the plausible deviations from the theory that will be discussed below. In any case, although both critical fields for F and B^k DW propagation have similar values for the presented arrays, the crossed-ratchet regime is reachable in the micrometer regime by facilitating the kink nucleation, which can be achieved by tilting the arrays with respect to the magnetisation EA.

3.3. Domain wall morphology and pinning

Knowledge on the small scale details of the DW morphology and pinning at the holes as well as the DW width is needed in order to understand the observed phenomenology in the global DW propagation across the asymmetric arrays, as well as to explain the deviations from the elastic theory calculations. Predictions from the model in Ref. [28] are built on infinitely narrow DWs. For a real sample, the requirement is fulfilled provided than the walls have a constant width and that their local curvature is always bigger that their width, which can easily obtained for hole sizes and separations much larger than the DW width. Besides, within this model, DWs must be perpendicular to any boundary, in particular to the sides of the holes. Magnetisation maps by means of XPEEM in portions of square arrays with $m_l = 4$ and holes of size $b = 500$ nm and 1 μm clearly show deviations from those two constraints.

First, from a XMCD image with two different domains, the DW width can be determined to be approximately 400 nm, as shown in Fig. 6 and in good agreement with estimations from Ref. [42]. In this situation the ratio domain wall width/hole size is such that the DW internal structure becomes important in determining DW pinning mechanism and, therefore, deviations from elastic theory model predictions should be expected. Second, one can readily see from Figs. 6 and 7 that DWs are not perpendicular to the hole perimeter at the contact points.[3]

DW to hole perimeter angles have been measured along the pinned DW from the experimental XMCD images, as sketched in Fig. 7 for a square array with $m_l = 4$ and $b = 500$ nm. Results are summarised in Table 1 and show two clear trends: first, nearly all obtained values are smaller than 90°; second, DW configuration is not symmetric in the top and bottom side of the holes. Average DW angle at the top side of the holes, $\alpha_{\text{top}} = 73°$, is clearly smaller than at their bottom side, $\alpha_{\text{bottom}} = 86°$.

It is therefore clear that the boundary conditions imposed in the elastic theory model are not valid for these arrays and that, to predict the interaction of the DW with

[3]Note that henceforward the EA and the base of the triangles is displayed as vertical.

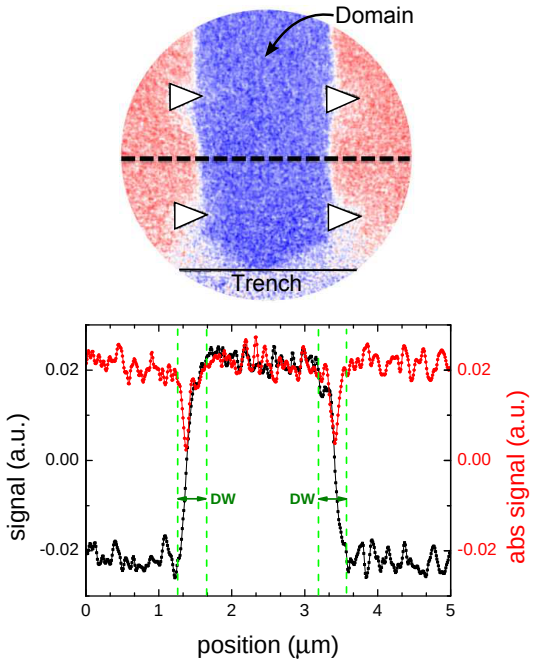

Figure 6: *Top:* XMCD image of a portion of the square array with $b = 1$ μm and $m_l = 4$. Red and blue colours indicate two different domains. Closure domains, in lighter colour, can be seen near the magnetic film boundaries (e.g. near the trench).The holes have been plotted on top of the image for the sake of clarity. *Bottom:* Plot of the signal in the XMCD image (black dots), mapped along the dashed line, and its absolute value (red dots).

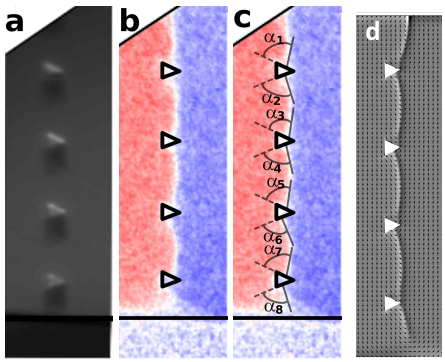

Figure 7: (a) XPEEM image of a row of triangles in the square array with $b = 500$ nm and $m_l = 4$. (b) Corresponding XMCD image -with the holes plotted on top- showing a pinned DW. (c) Illustration of the DW to hole perimeter angles summarised in Table 1. (d) DW configuration at forward depinning calculated by micromagnetic simulations for an array with the same geometrical dimensions.

the holes, more complicated models are needed, such as micromagnetic simulations that take into account the magneto-static energy. Indeed, DW configuration at forward depinning calculated by micromagnetic simulations confirm the experimental results in this array: DW

Table 1: DW angles at each side of each hole in the square array with $b = 500$ nm and $m_l = 4$ obtained from XMCD images and micromagnetic simulations. The error in the estimation of the angles from the XMCD images is ±3°.

	α_{top} (°)				α_{bottom} (°)			
	α_1	α_3	α_5	α_7	α_2	α_4	α_6	α_8
XMCD image	76	72	71	74	86	83	90	86
Mean		73				86		
Micromagnetic	71	65	65	65	87	75	77	88
Mean		66				82		

to hole intersection is never perpendicular and there is a clear asymmetry in the angles at top/bottom triangle sides, with an average difference, $\alpha_{bottom} - \alpha_{top} \approx 16°$, as shown in Fig. 7 and Table 1. Similar results are obtained for square arrays with $b = 500$ and $m_l = 3$ and 5 (see Table 2).

Table 2: Calculated DW angles at each side of each hole in square arrays with $b = 500$ nm obtained from micromagnetic simulations.

m_l	3	4	5
α_{top}	60° ± 7°	66° ± 3°	68° ± 3°
α_{bottom}	81° ± 5°	82° ± 7°	85° ± 2°
$\alpha_{bottom} - \alpha_{top}$	21°	16°	17°

It is interesting to note that the angle that would correspond to a flat wall parallel to the EA, $\alpha_{EA} = 90° - \theta = 63.5°$ (where θ was defined in Fig. 1), is close to the calculated α_{top}, in particular for the arrays with the smaller inter-hole distances. This indicates an enhanced DW stiffness, that hinders the DW to bend into a kinked configuration, thus explaining the suppression of kink DW propagation modes observed above.

A closer look at DW micromagnetic configuration near hole boundaries (Fig. 8(a)) allows to understand the asymmetries in the pinned DW shape. At the top hole perimeter, the 180° magnetisation rotation associated with the pinned DW corresponds to an edge half vortex with topological charge -1/2. At the bottom hole perimeter, the vacuum/magnetic material geometry is inverted and the DW-hole intersection corresponds to a +1/2 half vortex (for the opposite DW chirality +1/2 and -1/2 vortices would exchange places). Actually, a Néel DW segment pinned in between two holes is topologically equivalent by a 90° rotation to a transverse wall in a nanowire (which, in its simplest form, is composed of a pair of +1/2 and -1/2 half vortices at opposite nanowire edges[43, 44]). The different character of these fractional vortices, results in an asymmetric broadening of the pinned DW at top/bottom hole sides. These pertur-

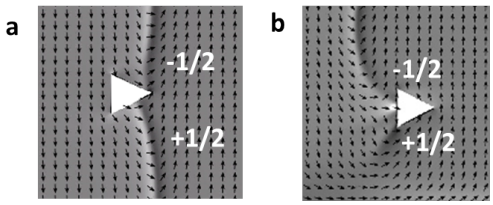

Figure 8: Detail of pinned DW close to a triangular hole, obtained by micromagnetic simulations. (a) Forward flat (F) DW propagation. (b) Backward flat (B) DW propagation. Note the different spin configuration at top/bottom hole perimeters due to the different sign of the fractional edge vortex in each case.

bations in the Néel DW internal structure extend into the magnetic film over a distance of the order of 300 nm/200 nm at the top/bottom hole perimeters, i.e. of the order of hole size $b = 500$ nm in this array. This results in a reduction of the effective "free" DW length that can bend under the pressure of the applied magnetic field and, therefore, in an enhancement of DW stiffness as inter-hole distances decrease.

Edge half vortex asymmetry is also at the root of the observed asymmetric pinned DW shape. This is illustrated in Fig. 8(b): in this image, the pinned DW has been pushed backwards by the pressure of a negative magnetic field to study the depinning process from the triangle bases. In this situation, in order to detach the pinned DW from the triangle hole, top/bottom DW endpoints should propagate along the triangle base: i.e. with the same edge geometry and under the effect of the same magnetic field. However, only the top -1/2 half vortex is able to propagate along the triangle base, whereas the bottom +1/2 half vortex remains pinned at the triangular hole apex. DW depinning takes place when the -1/2 half vortex travels all the way down along the triangle base and annihilates with the static +1/2 half vortex located at the bottom of the triangle. These differences in propagation mechanism for top/bottom DW ends become more relevant as hole size is reduced resulting in the observed asymmetric configuration of Fig. 7.

In summary, XMCD magnetic imaging and micromagnetic simulations show that DW morphology in the studied arrays is determined by the interplay between two different asymmetric factors. The first one is elastic DW bending under the effect of the applied field pressure, that reflects the asymmetry in the patterned triangular hole shape. This is the dominant factor in the 2D arrays of the large size regime in which crossed-ratchet effects had been observed.[17] The second factor is half vortex propagation along the edges of the triangular holes, which is one of the key issues in DW propagation in 1D nanowires.[24, 43, 44] This propagation is asymmetric due to the different topological charges at top/bottom DW ends and reflects the intrinsic asymmetry of a chiral Néel DW. Our results show that the small size regime in 2D arrays of asymmetric holes is marked by the asymmetry in pinned DW configurations and the enhancement of DW stiffness due to the increasing role of edge fractional vortices.

3.4. Current induced DW propagation

At this point, it is interesting to investigate the effects of a current on domain wall motion. We have performed micromagnetic simulations starting at a zero magnetisation state, with a Néel DW located in the middle of the array. Then, a ramp of electrical current has been applied in the forward/backward direction, from $j = 0$ to $3 \cdot 10^8 A/cm^2$. Some images have been extracted from the whole sequence and plotted in Fig. 9.

A clear asymmetry is observed in the DW propagation. For positive currents (meaning electrons propagating backward), the depinning of the DW in the B direction is observed at a current slightly above $j = 2 \cdot 10^8 A/cm^2$. For negative currents (electrons propagating forward), a factor 2 in j is necessary to achieve the depinning of the DW. These results suggest that the ratchet effect may not only exist in current induced DW motion but that it would be inverted respect to the magnetic field induced one, which might be related with a local increasing of j close to the triangle bases due to the hole symmetry.

The result from these simulations reveals a new route for the control of DWs in two opposite directions, each one with a different driving force (i.e. electrical currents

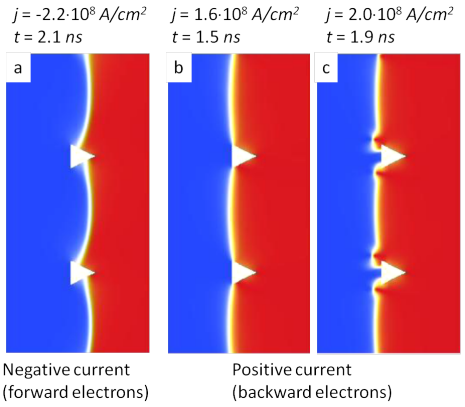

Figure 9: Micromagnetic simulations of a DW depinning by means of electrical currents in an array with $m_l = m_h = 4$, and holes of size $b = 500$ nm. (a) Forward DW propagation. (b,c) Backward DW propagation.

and magnetic fields), which could lead to the development of future domain-wall based devices.

4. Conclusions

In the search of an understanding of magnetic ratchet and crossed-ratchet effects, we have investigated 2D arrays of asymmetric holes exploring the micro and submicrometric range. On one hand, this small size regime was predicted to be the optimum size for the observation of these effects. On the other, it also corresponds to the existing gap in the literature between point-like DWs in nanowires and the elastic DW lines in 2D arrays of holes in the large size regime.

We show that both the ratchet and crossed-ratchet effects are experimental reachable for 2D arrays in the small size regime, where DWs and holes are comparable in size. However, the occurrence of crossed-ratchet effects has been demonstrated to be less frequent than the predictions made by theory and simulations. Indeed, flat DWs walls are favoured and switching processes take place through those walls propagating in the forward direction for arrays aligned with the EA of the magnetic film, while for the tilted arrays both F and B^k propagation take place at the same field. In any case, the fabrication of arrays tilted with respect to the EA has been proven to be a successful route for kink nucleation that then propagates in the B^k direction.

Critical fields for kinked backward DW propagation H_B^k and flat forward propagations H_F have been seen to be closer that anticipated. Although the large contribution of the coercive field of the film to both propagation fields has an influence in their ratio, there is an additional hardening of kink propagation modes in comparison with predictions from elastic theory models. This has been confirmed with XPEEM high resolution magnetic images of the DWs in the proximity of the triangular holes as well as with micromagnetic simulations. Similarly to what has been studied in magnetic nanowires, the role of half vortices -located at hole edges- becomes increasingly important to determine pinned DW configurations as hole size becomes comparable to DW width. This results in stiffer DWs with asymmetric shapes that mark the small size regime, which should be considered when designing future devices based on 2D arrays.

Additionally, micromagnetic simulations suggest an inverted ratchet effect for current induced DW propagation, opening the door to an alternative road for achieving the crossed-ratchet regime in small size hole arrays. This offers a promising candidate for novel devices where DW propagation in two opposite directions can be controlled with electrical currents and magnetic fields; all this occurring at the sub-micrometric range.

Acknowledgments

The financial support of the Spanish MINECO MAT2014-53921-R, FIS2013-45469 and FIS2016-76058 (AEI) and the Aragonese DGA IMANA E34 and CAMRADS E69, all of them cofunded by Fondo Social Europeo and European Union FEDER funds, is acknowledged. A. H-R acknowledges the support from FCT of Portugal (Grant SFRH/BPD/90471/2012)

References

[1] S. S. P. Parkin, M. Hayashi, L. Thomas, Magnetic Domain-Wall Racetrack Memory, Science 320 (5873) (2008) 190–194. doi:10.1126/science.1145799.

[2] D. Atkinson, D. S. Eastwood, L. K. Bogart, Controlling domain wall pinning in planar nanowires by selecting domain wall type and its application in a memory concept, Appl. Phys. Lett. 92 (2) (2008) 022510. doi:10.1063/1.2832771.

[3] S. E. Barnes, J. Ieda, S. Maekawa, Magnetic memory and current amplification devices using moving domain walls, Appl. Phys. Lett. 89 (12) (2006) 122507. doi:10.1063/1.2354036.

[4] D. A. Allwood, G. Xiong, C. C. Faulkner, D. Atkinson, D. Petit, R. P. Cowburn, Magnetic Domain-Wall Logic, Science 309 (5741) (2005) 1688–1692. doi:10.1126/science.1108813.

[5] P. Xu, K. Xia, C. Gu, L. Tang, H. Yang, J. Li, An all-metallic logic gate based on current-driven domain wall motion, Nat. Nano 3 (2) (2008) 97–100. doi:10.1038/nnano.2008.1.

[6] D. A. Allwood, G. Xiong, M. D. Cooke, C. C. Faulkner, D. Atkinson, N. Vernier, R. P. Cowburn, Submicrometer Ferromagnetic NOT Gate and Shift Register, Science 296 (5575) (2002) 2003–2006. doi:10.1126/science.1070595.

[7] X. Zhou, Z. Huang, W. Zhang, Y. Yin, P. Dürrenfeld, S. Dong, Y. Zhai, Current-induced multiple domain wall motion modulated by magnetic pinning in zigzag shaped nanowires, AIP Advances 7 (5) (2017) 056014. doi:10.1063/1.4975129.

[8] O. Gomonay, M. Kläui, J. Sinova, Manipulating antiferromagnets with magnetic fields: Ratchet motion of multiple domain walls induced by asymmetric field pulses, Applied Physics Letters 109 (14) (2016) 142404. doi:10.1063/1.4964272.

[9] J. Cui, S. M. Keller, C.-Y. Liang, G. P. Carman, C. S. Lynch, Nanoscale magnetic ratchets based on shape anisotropy, Nanotechnology 28 (8) (2017) 08LT01. doi:10.1088/1361-6528/aa56d4.

[10] D. A. Allwood, G. Xiong, R. P. Cowburn, Domain wall diodes in ferromagnetic planar nanowires, Appl. Phys. Lett. 85 (14) (2004) 2848–2850. doi:10.1063/1.1802388.

[11] M. T. Bryan, T. Schrefl, D. A. Allwood, Symmetric and asymmetric domain wall diodes in magnetic nanowires, Appl. Phys. Lett. 91 (14) (2007) 142502. doi:10.1063/1.2794030.

[12] J. H. Franken, H. J. M. Swagten, B. Koopmans, Shift registers based on magnetic domain wall ratchets with perpendicular anisotropy, Nat. Nano. 7 (8) (2012) 499–503. doi:10.1038/nnano.2012.111.

[13] M. Hayashi, L. Thomas, R. Moriya, C. Rettner, S. S. P. Parkin, Current-Controlled Magnetic Domain-Wall Nanowire Shift Register, Science 320 (5873) (2008) 209–211. doi:10.1126/science.1154587.

[14] J. R. Whyte, J. M. Gregg, A diode for ferroelectric domain-wall motion, Nature Communications 6 (2015) 7361. doi:10.1038/ncomms8361.

[15] X. Ma, C. J. O. Reichhardt, C. Reichhardt, Reversible vector ratchets for skyrmion systems, Phys. Rev. B 95 (2017) 104401. doi:10.1103/PhysRevB.95.104401.

[16] B. Chesca, D. John, R. Pollett, M. Gaifullin, J. Cox, C. J. Mellor, S. Savel'ev, Magnetic field tunable vortex diode made of yba2cu3o7 josephson junction asymmetrical arrays, Applied Physics Letters 111 (6) (2017) 062602. doi:10.1063/1.4997741.

[17] A. Pérez-Junquera, V. I. Marconi, A. B. Kolton, L. M. Álvarez-Prado, Y. Souche, A. Alija, M. Vélez, J. V. Anguita, J. M. Alameda, J. I. Martín, J. M. R. Parrondo, Crossed-Ratchet Effects for Magnetic Domain Wall Motion, Phys. Rev. Lett. 100 (3) (2008) 037203. doi:10.1103/PhysRevLett.100.037203.

[18] J.-S. Kim, O. Boulle, S. Verstoep, L. Heyne, J. Rhensius, M. Kläui, L. J. Heyderman, F. Kronast, R. Mattheis, C. Ulysse, G. Faini, Current-induced vortex dynamics and pinning potentials probed by homodyne detection, Phys. Rev. B 82 (10) (2010) 104427. doi:10.1103/PhysRevB.82.104427.

[19] N. Kheirabadi, E. McCann, V. I. Fal'ko, Magnetic ratchet effect in bilayer graphene, Phys. Rev. B 94 (2016) 165404. doi:10.1103/PhysRevB.94.165404.

[20] G. V. Budkin, L. E. Golub, E. L. Ivchenko, S. D. Ganichev, Magnetic ratchet effects in a two-dimensional electron gas, JETP Letters 104 (9) (2016) 649. doi:10.1134/S0021364016210074.

[21] S. Savel'ev, A. Rakhmanov, F. Nori, Experimentally realizable devices for domain wall motion control, New J. Phys. 7 (1) (2005) 82. doi:10.1088/1367-2630/7/1/082.

[22] H.-G. Piao, H.-C. Choi, J.-H. Shim, D.-H. Kim, C.-Y. You, Ratchet effect of the domain wall by asymmetric magnetostatic potentials, Appl. Phys. Lett. 99 (19) (2011) 192512. doi:10.1063/1.3658805.

[23] S.-G. Je, D.-H. Kim, S.-C. Yoo, B.-C. Min, K.-J. Lee, S.-B. Choe, Asymmetric magnetic domain-wall motion by the Dzyaloshinskii-Moriya interaction, Phys. Rev. B 88 (21) (2013) 214401. doi:10.1103/PhysRevB.88.214401.

[24] D. Bedau, M. Kläui, M. T. Hua, S. Krzyk, U. Rüdiger, G. Faini, L. Vila, Quantitative Determination of the Nonlinear Pinning Potential for a Magnetic Domain Wall, Phys. Rev. Lett. 101 (25) (2008) 256602. doi:10.1103/PhysRevLett.101.256602.

[25] A. Himeno, S. Kasai, T. Ono, Current-driven domain-wall motion in magnetic wires with asymmetric notches, Appl. Phys. Lett. 87 (24) (2005) 243108. doi:10.1063/1.2140884.

[26] A. Alija, A. Pérez-Junquera, G. Rodríguez-Rodríguez, M. Vélez, V. I. Marconi, A. B. Kolton, J. V. Anguita, J. M. Alameda, J. M. R. Parrondo, J. I. Martín, Domain wall energy landscapes in amorphous magnetic films with asymmetric arrays of holes, J. Phys. D: Appl. Phys. 42 (4) (2009) 045001. doi:10.1088/0022-3727/42/4/045001.

[27] A. Alija, A. Hierro-Rodríguez, A. Pérez-Junquera, J. M. Alameda, J. I. Martín, M. Vélez, Crossed ratchet effects on magnetic domain walls: geometry and transverse field effects, J. Phys. D: Appl. Phys. 44 (32) (2011) 325002. doi:10.1088/0022-3727/44/32/325002.

[28] V. I. Marconi, A. B. Kolton, J. A. Capitán, J. A. Cuesta, A. Pérez-Junquera, M. Vélez, J. I. Martín, J. M. R. Parrondo, Crossed-ratchet effects and domain wall geometrical pinning, Phys. Rev. B 83 (21) (2011) 214403. doi:10.1103/PhysRevB.83.214403.

[29] M. Vélez, C. Mény, S. M. Valvidares, J. Díaz, R. Morales, L. M. Alvarez-Prado, P. Panissod, J. M. Alameda, Amorphous to polycrystalline transition in coxsi(1-x) alloy thin films, Eur. Phys. J. B 41 (4) (2004) 517. doi:10.1140/epjb/e2004-00345-0.

[30] C. Castán Guerrero, On holes and walls: Tailoring the magnetic properties of thin films through 2D nanopatterning, Vol. 118 of Colección Estudios de Física, Prensas de la Universidad de Zaragoza, 2015.

[31] K. J. Merazzo, C. Castán-Guerrero, J. Herrero-Albillos, F. Kronast, F. Bartolomé, J. Bartolomé, J. Sesé, R. P. del Real, L. M. García, M. Vázquez, X-ray photoemission electron microscopy studies of local magnetization in py antidot array thin films, Phys. Rev. B 85 (2012) 184427. doi:10.1103/PhysRevB.85.184427.

[32] M. Donahue, D. Porter, OOMMF User's Guide, Version 1.0, Interagency Report NISTIR 6376. National Institute of Standards and Technology, Gaithersburg, MD; http://math.nist.gov/oommf. (1999).

[33] C. Castán-Guerrero, J. Herrero-Albillos, J. Bartolomé, F. Bartolomé, L. A. Rodríguez, C. Magén, F. Kronast, P. Gawronski, O. Chubykalo-Fesenko, K. J. Merazzo, P. Vavassori, P. Strichovanec, J. Sesé, L. M. García, Magnetic antidot to dot crossover in Co and Py nanopatterned thin films, Phys. Rev. B 89 (14) (2014) 144405. doi:10.1103/PhysRevB.89.144405.

[34] H. Tanigawa, T. Koyama, M. Bartkowiak, S. Kasai, K. Kobayashi, T. Ono, Y. Nakatani, Dynamical pinning of a domain wall in a magnetic nanowire induced by walker breakdown, Phys. Rev. Lett. 101 (2008) 207203. doi:10.1103/PhysRevLett.101.207203.

[35] U.-H. Pi, Y.-J. Cho, J.-Y. Bae, S.-C. Lee, S. Seo, W. Kim, J.-H. Moon, K.-J. Lee, H.-W. Lee, Static and dynamic depinning processes of a magnetic domain wall from a pinning potential, Phys. Rev. B 84 (2011) 024426. doi:10.1103/PhysRevB.84.024426.

[36] A. Hubert, R. Schäfer, Magnetic Domains, Springer, Berlin, 1998.

[37] D. A. D. M. Burn, Effective pinning energy landscape perturbations for propagating magnetic domain walls, Scientific Reports 6 (2016) (34517). doi:10.1038/srep34517.

[38] T. J. Hayward, Intrinsic nature of stochastic domain wall pinning phenomena in magnetic nanowire devices, Scientific Reports 5 (2015) 13279. doi:10.1038/srep13279.

[39] J. P. M. Moñoz, Suppression of the intrinsic stochastic pinning of domain walls in magnetic nanostripes, Nat.Commun. (2011) 2 (562). doi:10.1038/ncomms15752011.

[40] J. Briones, F. Montaigne, M. Hehn, D. Lacour, J. R. Childress, M. J. Carey, Stochastic and complex depinning dynamics of magnetic domain walls, Phys. Rev. B 83 (2011) 060401. doi:10.1103/PhysRevB.83.060401.

[41] M.-Y. Im, L. Bocklage, P. Fischer, G. Meier, Direct observation of stochastic domain-wall depinning in magnetic nanowires, Phys. Rev. Lett. 102 (2009) 147204. doi:10.1103/PhysRevLett.102.147204.

[42] A. Pérez-Junquera, G. Rodríguez-Rodríguez, M. Vélez, J. I. Martín, H. Rubio, J. M. Alameda, Néel wall pinning on amorphous coxsi1x and coyzr1y films with arrays of antidots in the diluted regime, J. Appl. Phys. 99 (3) (2006) 033902. doi:10.1063/1.2161801.

[43] O. Tchernyshyov, G.-W. Chern, Fractional Vortices and Composite Domain Walls in Flat Nanomagnets, Phys. Rev. Lett. 95 (19) (2005) 197204. doi:10.1103/PhysRevLett.95.197204.

[44] A. Pushp, T. Phung, C. Rettner, B. P. Hughes, S.-H. Yang, L. Thomas, S. S. P. Parkin, Domain wall trajectory determined by its fractional topological edge defects, Nat. Phys. 9 (8) (2013) 505–511. doi:10.1038/nphys2669.

SUPPLEMENTARY MATERIAL.
2D magnetic domain wall ratchet: the limit of submicrometric holes

J. Herrero-Albillos, C. Castán-Guerrero, F. Valdés-Bango, J. Bartolomé, F. Bartolomé, F. Kronast,
A. Hierro-Rodriguez, L. M. Álvarez Prado, J. I. Martín, M. Vélez, J. M. Alameda, J. Sesé, L. M. García

Flat domain wall propagation

In this link, a video of a flat wall propagating forward can be watched. The geometrical parameters are the same as in Fig 3 of the mail text (e.g. with b = 500 nm, m_l = 5, m_h = 3 and triangles pointing upwards).

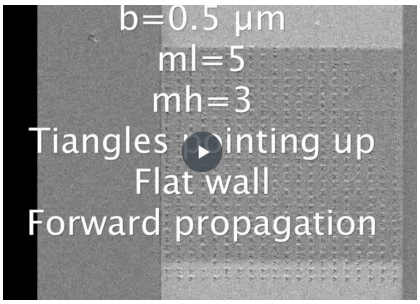

Figure 1: Snapshot from the video of a flat wall moving F (up).

In Fig. 2(a), an XPEEM image of an area of 3x3 holes in the bottom-right corner of an array with b = 1 μm, $m_l = m_h$ = 4 is shown. One of the trenches can be seen in the bottom of the image. XMCD images have been recorded with a larger zoom in the two regions limited by dashed lines. The frame color of each image indicates the region at which it corresponds.

In (c) a blue (negative magnetisation) domain is confined by two DWs (labelled as 1 and 2) pinned at two columns of holes, at a 0 magnetic applied field. When a negative magnetic field is applied, the blue domain tends to grow, pushing the DWs out. At a higher applied field (d) both DWs have moved slightly through the holes. When the field is further increased (e), DW #1 has enough energy to overcome the pinning of the holes, propagating to the continuous film in the direction defined as F. DW #2, however, remains pinned and does not propagate in the B direction, indicating a ratchet effect. In (f), an XMCD image is taken in the region surrounded in (a) by a green dashed line. Thus,

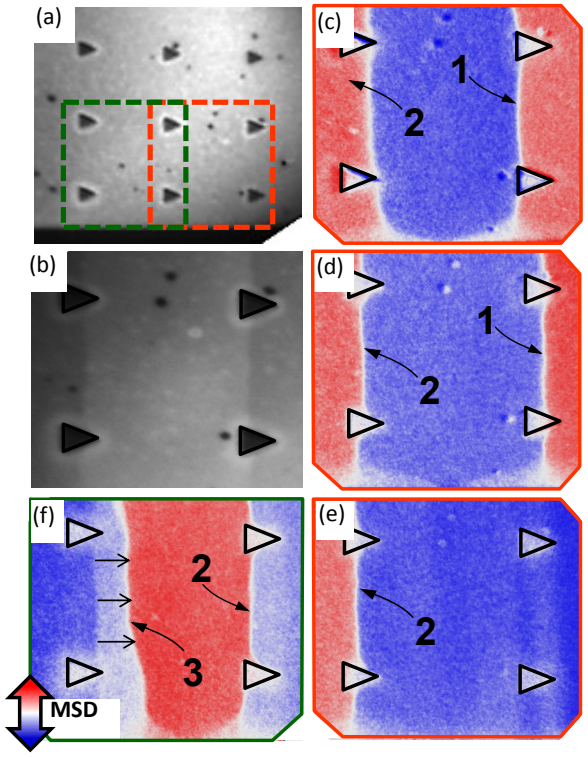

Figure 2: (Colour online) (a) XPEEM image of a corner of the array of triangle-shaped holes with b = 1 μm, $m_l = m_h$ = 4, oriented parallel to the E.A. The array is limited by the trench below and the continuous film to the right. (b) XPEEM image corresponding to the area covered by the orange rectangle in (a). (c to f) XMCD images have been recorded at increasing magnetic fields. (c), (d), and (e) correspond to the red rectangle, (f) to the green rectangle. Three different DW can be seen in the sequence (indicated with a number) moving F, i.e. to the right in the images. DW #2 can be seen in all of the images. Black lines have been drawn to locate the borders of the holes.

the right DW in this image is the DW 2 that remained pinned in image (e). DW #2 has moved towards the base of the triangles and remained there. A third DW (labelled as 3) has crossed the entire array from its left

side in the F direction. DW #3 has depinned from the left column of holes and moved in F direction during measurement, as indicated by the arrows.

This image sequence shows that the origin of ratchet effect for flat DW propagation lies in the difficulty of the DWs to depin from the base of the triangle-shaped holes, in comparison with depinning from their endpoints. Actually, micro-magnetic simulations of forward (H_F) and backward (H_B) propagation fields for a flat DW across an array with similar geometry give an asymmetry ratio $H_F/H_B = 0.5$ caused by the stronger DW bending needed to depin from triangle bases. Further discussion on the results from micro-magnetic simulations are presented in the main text. In this link a video of a micro-magnetic simulation with a DW moving forward can be watched.

Flat domain wall propagation in symmetric holes

In order to prove that only the shape of the holes is inducing the ratchet effect, one array has been fabricated with symmetric hole shape respect to the DW propagation direction. Each hole is a rhomb, composed of two triangles joined at the base, as depicted in Fig. 3. The parameters of the array are $b = 500$ nm and $m_l = m_h = 4$. The array was produced in the same substrate as the arrays of triangles, following the procedure as described in the main text.

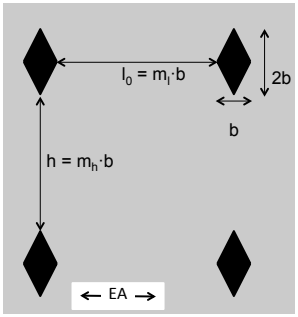

Figure 3: Scheme of the geometrical parameters for the arrays of symmetric holes.

Kerr microscopy images of the DW propagation through the array are shown in Fig. 4. The image quality is lower than in the triangle-shaped hole arrays because the distortion caused by the holes is larger, however DWs can still be appreciated. The black dashed lines indicate the DW position and the red arrows indicate their propagation direction. Black rectangles at both sides of the array indicate the position of the trench.

It can be clearly observed that the two DWs are moving towards each other in opposite directions, showing no preferred propagation direction and therefore no ratchet effect. The equivalent array with triangular holes does show clear ratchet effect, as discussed in the main text.

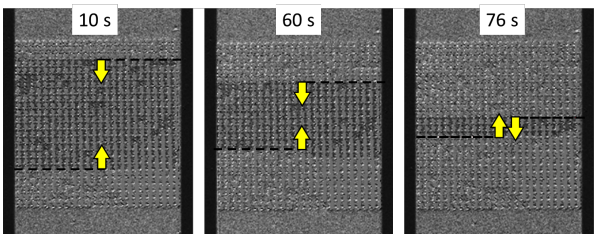

Figure 4: (Color online) Kerr microscopy images at different times during the DW propagation in the array of rhomb-shaped holes. Dashed lines and yellow arrows indicate the DW position and propagation direction, respectively.

1. Kink domain wall propagation

A video of the Kerr microscopy experiments carried in an array tilted 13° with respect to the EA with $b = 1\mu$m, $m_l = m_h = 3$ and triangles pointing up can be watched in this link. B_k at the top of the array can be easily distinguish as the light/dark grey contrast moves from left to right in only one row at a time. F propagation occurs following the direction marked by the EA. Data had been already presented and discussed in detail in subsection 3.2 of the main text.

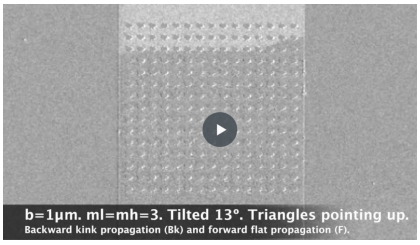

Figure 5: Snapshot from the video of a kinked wall moving B (down) and a flat wall moving F (up) for an array tilted 13° with respect to the EA with $b = 1$ μm, $m_l = m_h = 3$ and triangles pointing up.

A similar video, for holes with $b = 500$ is presented in this link. Although the visualisation of kinks is more challenging due to the limited resolution of the microscope, flat and and kinked domain wall propagation can be also identified as in the previous video.

In Fig. 7, selected images form the previous video are shown as a function of time, where a the central domain with clear grey tone is limited by two DWs, that

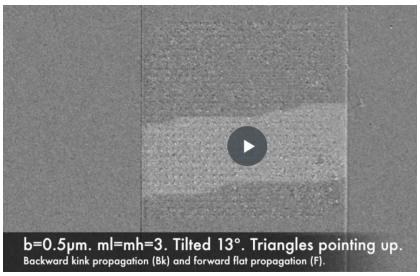

Figure 6: Snapshot from the video of a kinked wall moving B (down) and a flat wall moving F (up) for an array tilted 13° with respect to the EA with b = 500 mm, $m_l = m_h = 3$ and triangles pointing up.

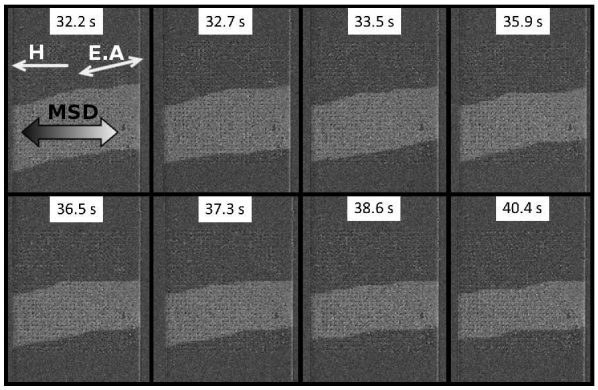

Figure 7: Selected photograms corresponding to the crossed-ratchet regime of DW propagation in the array 13° tilted, with b = 500 nm, $m_l = m_h = 3$ and triangles pointing up, under a constant magnetic field of -7.3 Oe.

propagate towards each other in order to complete the switching process. As the DWs are tilted with respect to the array period, they suffer an inhomogeneous pinning by the holes. According to that, the DW at the bottom is not flat, though the overall movement is in the direction perpendicular to the E.A., i.e. forward. In contrast, the top DW propagation occurs through kinks moving from left to right, i.e. B_k.

This is more clearly visualised in Fig. 8, where a grey-scale picture of the progress of the central domain as a function of time is shown. Here, pictures of the central domain at different times have been superimposed. Time is indicated by the color, from black to white. The direction of propagation of the DWs is given by the tone gradient. Yellow stars indicate the points at which a kink starts propagating to the right side of the array, that is, in the B_k direction. The experiments performed in this array suggest that DWs propagate forward through flat mode (F), and backward through kinked mode (B_k), which means that the crossed-ratchet regime has been observed for this array as well.

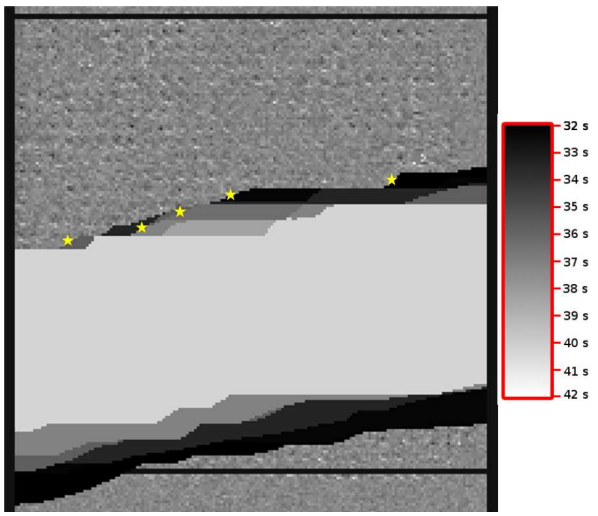

Figure 8: (Colour online) Grey-scale picture of the progress of the central domain as a function of time in the crossed-ratchet regime, in the array 13° tilted with respect to the easy axis, with b = 500 nm, $m_l = m_h = 3$ and triangles pointing up, under a constant magnetic field of -7.3 Oe.

2. Current induced DW propagation

Follow this link for the video of micro-magnetic simulations of the ratchet effect on current induced DW motion already discussed in the main text.

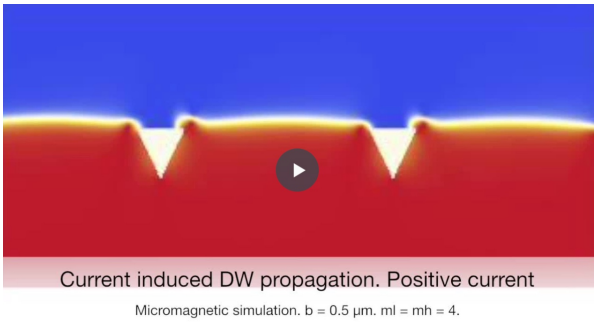

Figure 9: (Colour online) Snapshot from the video of micro-magnetic simulations of a DW depinning by means of electrical currents in an array with $m_l = m_h = 4$, and holes of size b = 500 nm.